Simulations of multiple scattering by tree trunks using the TLM method

P. Chobeau[a], D. Ecotière[a], G. Dutilleux[a] et J. Picaut[b]
[a]LRPC de Strasbourg, 11 rue Jean Mentelin, 67000 Strasbourg, France
[b]Ifsttar Nantes LAE, Route de Bouaye CS4, 44344 Bouguenais, France
pierre.chobeau.etu@univ-lemans.fr

The transmission-line matrix (TLM) method has recently been updated for the simulation of outdoor sound propagation. In this framework, sound propagation through forest is currently studied using the TLM method. Multiple scattering caused by tree-trunks is one of the three main phenomena encountered inside forested area which can significantly influence sound wave propagation. This paper presents the TLM simulations related to both single and multiple scattering, where every numerical results are compared to analytical solutions. For every multiple scattering simulations, the scatterers' locations are related to the distribution processes used in spatial forest structure analysis. Correct agreement are found between the numerical results and the analytical solutions, which would constitute a first step for the TLM method validation in the vicinity of forest.

1 Introduction

Sound propagation through forest is mainly influenced by the three following phenomena: low-frequency absorption from ground effect, sound scattering by tree-trunks and sound fluctuations caused by the local meteorological effects. A good introduction to each one of these acoustic phenomena occurring when a sound wave travels inside forests can be found in [1, 2, 3]. Among these, the sound scattering by tree trunks is considered to be significant when the frequency of the acoustic waves is close to the apparent diameter of the trunks. Interactions between scattered sound waves could give rise to constructive or destructive interferences for example. This would impact directly the sound level predictions in the vicinity of forests.

The influence of sound scattering is investigated using the transmission-line matrix (TLM) method. This time-domain method enables to simulate acoustic propagation in medium related to outdoor sound propagation [4]. The theory related to the TLM method is reminded in the next section. The third section presents 2D-simulations carried out with a single scatterer. Each of the following TLM simulations are compared to analytical solutions and can be considered as a first validation step in the study of multiple scattering. In the forth section, multiple scattering from 2D circular scatterers is investigated from the TLM simulations and compared to analytical solutions.

2 The TLM method for acoustics

The TLM method simulates wave propagation of pressure pulses inside a spatial mesh where pressure pulses travel from a node to its neighbors through transmission lines [5]. Incident pulses ${}_tI^n_{(i,j)}$ and scattered pulses ${}_tS^m_{(i,j)}$ for a given node position (i, j) are depicted by figure 1. Indexes n and m correspond to the number of the branch where pulses are traveling. Incident and scattered pulses can be put into vectors as follow:

$$ {}_t\mathbf{I}_{(i,j)} = [\,{}_tI^1;\ {}_tI^2;\ {}_tI^3;\ {}_tI^4]^T_{(i,j)}, \quad (1) $$

$$ {}_t\mathbf{S}_{(i,j)} = [\,{}_tS^1;\ {}_tS^2;\ {}_tS^3;\ {}_tS^4]^T_{(i,j)} \quad (2) $$

where (i, j) corresponds to the node position in the discretized TLM network and the exponent T denotes the transposed of the original vectors ${}_t\mathbf{I}_{(i,j)}$ and ${}_t\mathbf{S}_{(i,j)}$. The scattering process for each node of the transmission-line network is written as:

$$ {}_t\mathbf{S}_{(i,j)} = {}_t\mathbf{D}_{(i,j)}\ {}_t\mathbf{I}_{(i,j)}\ , \quad (3) $$

where ${}_t\mathbf{D}_{(i,j)}$ is the scattering matrix which gives the proportion of reflected and transmitted pulses at every node of the TLM network.

In the case of outdoor sound propagation, physical phenomena such as atmospheric turbulence induce heterogeneities of the propagation medium. Atmospheric absorption induces additional dissipation which should be taken into account in the model. Both phenomena are implemented in the TLM method through the introduction of specific additional branches.

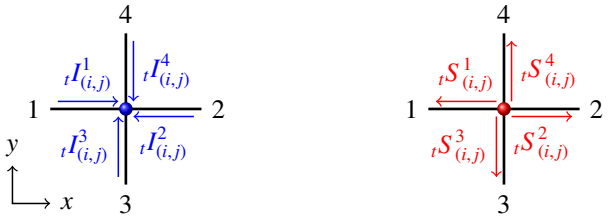

Figure 1: Incident ${}_tI^n_{(i,j)}$ and scattered ${}_tS^m_{(i,j)}$ pulses for a node (i, j) at the time t for an homogeneous and non dissipative medium (2D).

Heterogeneities

It has been shown [6] that an additional branch at each node can be used to set the local sound celerity. This approach introduces the parameter η that allows to modify the local impedance through an additional fifth branch of length $\delta l/2$. This branch presents a characteristic impedance Z_0/η (see Fig. 2), where Z_0 corresponds to the characteristic impedance of the main branches.

Dissipation

Dissipation phenomena can be simulated for a given frequency by adding a branch. This branch presents an anechoic termination and a specific impedance Z_0/ζ. As the termination of the dissipation's branch is anechoic, the wave that travels in such a branch is neither transmitted nor reflected.

Therefore, to simulate acoustic propagation in an heterogeneous and dissipative medium the TLM network has to be modified as shown in figure 2, which gives rise to five incident and scattered pulses.

$$ {}_t\mathbf{I}_{(i,j)} = [\,{}_tI^1;\ {}_tI^2;\ {}_tI^3;\ {}_tI^4;\ {}_tI^5]^T_{(i,j)}, \quad (4) $$

$$ {}_t\mathbf{S}_{(i,j)} = [\,{}_tS^1;\ {}_tS^2;\ {}_tS^3;\ {}_tS^4;\ {}_tS^5]^T_{(i,j)}, \quad (5) $$

where ${}_tI^5$ and ${}_tS^5$ corresponds to incident and scattered pulses from the additional fifth branch which aims at introducing heterogeneities in the transmission-line network.

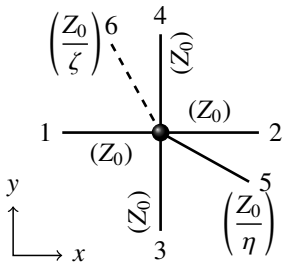

Figure 2: Additional branches for acoustic propagation in an heterogeneous and dissipative medium (2D).

The superposition principle allows to write the pressure at a given node position as follows:

$$ {}_tp_{(i,j)} = \frac{2}{\eta_{(i,j)} + \zeta_{(i,j)} + 4} \left[\sum_{n=1}^{4} {}_tI^n_{(i,j)} + \eta_{(i,j)}\ {}_tI^5_{(i,j)} \right]. \quad (6) $$

At a given node position (i, j), each scattered pulse ${}_tS^m$ travel along the discretized distance δl during the time δt and becomes an incident pulse ${}_{t+\delta t}I^n$ at an adjacent node. For the node position (i, j), this is written as:

$$ {}_{t+\delta t}I^1_{(i,j)} = {}_tS^2_{(i-1,j)}, \quad (7a) $$

$$ {}_{t+\delta t}I^2_{(i,j)} = {}_tS^1_{(i+1,j)}, \quad (7b) $$

$$ {}_{t+\delta t}I^3_{(i,j)} = {}_tS^4_{(i,j-1)}, \quad (7c) $$

$$ {}_{t+\delta t}I^4_{(i,j)} = {}_tS^3_{(i,j+1)}. \quad (7d) $$

$$ {}_{t+\delta t}I^5_{(i,j)} = {}_t S^5_{(i,j)}. \quad (7e) $$

From the combination of the matrix relation, the connexion laws and the nodal pressure definition, the iterative schemes for heterogeneous and dissipative TLM network is written as:

$$ \begin{aligned} {}_{t+\delta t}p_{(i,j)} = & \frac{2}{\eta_{(i,j)} + \zeta_{(i,j)} + 4} [\ {}_tp_{(i+1,j)} + {}_tp_{(i-1,j)} \\ & + {}_tp_{(i,j+1)} + {}_tp_{(i,j-1)} + \eta_{(i,j)}\ {}_tp_{(i,j)}] \\ & - \frac{\eta_{(i,j)} - \zeta_{(i,j)} + 4}{\eta_{(i,j)} + \zeta_{(i,j)} + 4}\ {}_{t-\delta t}p_{(i,j)}\ , \end{aligned} \quad (8) $$

where time and spatial derivatives can be identified to give the wave following wave equation:

$$ \left[\left(\frac{\partial^2}{\partial x^2} + \frac{\partial^2}{\partial y^2} \right) - \frac{\eta + 4}{2} \frac{\delta t^2}{\delta l^2} \frac{\partial^2}{\partial t^2} - \zeta \frac{\delta t}{\delta l^2} \frac{\partial}{\partial t} \right] {}_tp_{(i,j)} = 0\ . \quad (9) $$

3 Scattering of a plane wave by a single cylinder

3.1 Theory

The propagation of a monochromatic acoustic wave in the vicinity of a circular scatterer with a radius a in a cylindrical coordinate system (r, φ, z) can be written as the sum of cylindrical waves as follows [7]:

$$ p_i = P_0 \sum_{m=0}^{\infty} (2 - \delta_{m0}) i^m\ J_m\ (kr)\ e^{im\varphi}\ e^{i\omega t}, \quad (10) $$

where k is the wave number, ω the angular frequency, P_0 the amplitude of the incident wave, δ_{m0} the Dirac function and J_m is the Bessel function of the first kind for real order m. The scattered wave is written as divergent cylindrical wave

$$ p_s = P_0 \sum_{n=0}^{\infty} A_n H_n^{(1)}\ (kr)\ e^{in\varphi}\ e^{i\omega t}, \quad (11) $$

where $H_n^{(1)}$ is the Hankel function of the first kind for real order n. The coefficients A_n are derived from the boundary condition which can be written at $r = a$:

$$ \frac{i}{k\rho c} \frac{\partial}{\partial r} (p_i + p_s) = \frac{-1}{Z} (p_i + p_s), \text{ for } r = a, \quad (12) $$

where Z is the normal acoustic impedance of the cylinder, ρ is the mass density and c the sound speed in the air. Thus, the coefficients A_n can be written as [7]:

$$ A_n = -\frac{(2 - \delta_{n0}) i^n [i J_n'(ka) + (\rho c/Z) J_n(ka)]}{i H_n^{(1)'}(ka) + (\rho c/Z) H_n^{(1)}(ka)}. \quad (13) $$

Through this coefficient A_n, the surface impedance of the cylinder can be taken into account.

3.2 Principle and geometries

3.2.1 Instantaneous pressure fields

Figure 3 shows the geometry of the numerical model where a monochromatic plane wave of frequency $f = 100$ Hz coming from the left hit a perfectly rigid cylinder. The top, bottom and left boundaries are considered as perfectly rigid whereas the right boundary is made of an absorbing layer. The simulation duration is set to not allow the scattered wave to hit the boundaries. The difference in magnitude of the

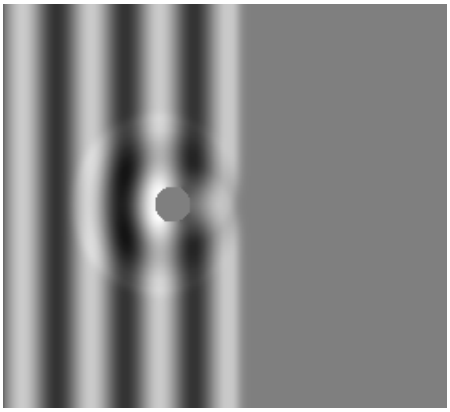

Figure 3: Distribution of pressure magnitude from the TLM model: scattering of rigid cylinder with a monochromatic plane wave incidence.

instantaneous pressure are depicted by different gray levels, where the intermediate gray shade represents zero whereas the darker and brighter shows respectively the minimal and maximal pressure magnitudes.

3.2.2 Geometries and calculation process

TLM calculations are carried out in two main steps: first, TLM simulations are performed without cylinder for a given monochromatic excitation in the computation domain depicted by figure 4. This first step gives the

incident pressure field which root mean square value: $p_{i,\mathrm{rms}}$, is calculated at every receiver position. The second step consists in running TLM simulations with the cylinder and the same excitation signal (see Fig. 4). This second step gives the total pressure field, i.e. the incident and scattered pressure fields. Finally, subtracting the incident pressure field of the first simulation from the total pressure field of the second simulation gives the scattered pressure field p_s for every simulation. The root mean square scattered pressure is calculated from the scattered field $p_{s,\mathrm{rms}}$ over four periods at every receiver placed around the cylinder as depicted in figure 4. The sound level pressure L_{scat} (in dB) of the scattered field relative to the incident field obtained from the TLM calculation is given by:

$$L_{\mathrm{scat}} = 10\log_{10}\left(\frac{p_{s,\mathrm{rms}}}{p_{i,\mathrm{rms}}}\right), \tag{14}$$

where $p_{s,\mathrm{rms}}$ and $p_{i,\mathrm{rms}}$ are respectively the scattered and incident root mean square pressures.

The source signal corresponds to a monochromatic plane wave which frequency is set at a given value for every simulation. The cylinder diameter and location are fixed at the same values for every simulation. This allows to repeat the simulations with exactly the same geometrical configuration for several frequencies. In order to look at a range of ka that is significantly large, the frequency of the source signal is taken in the frequency range [200 - 1600] Hz. In the following TLM simulations the cylinder is located

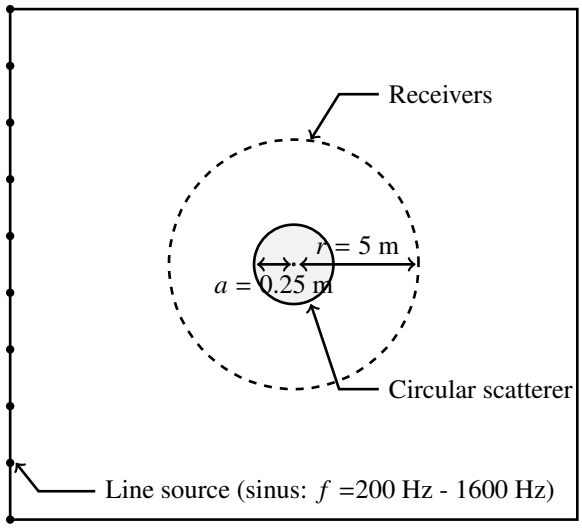

Figure 4: *Computational domain of the TLM simulations for the calculation of the pressure field scattered by a circular and acoustically rigid scatterer.*

in the center of the computational domain, the radius of the cylinder is: $a = 0.25$ m and the distance between the center of the cylinder and every receiver $r = 5$ m. The simulations duration is set to not exceed 0.06 s, which does not allow the scattered field to reach the boundary of the computational domain for every simulation. This simulation duration enables to get at least four time periods of the source signal at every receiver for averaging the pressure field to calculate the root mean square pressure of both incident and scattered fields.

3.3 Comparisons between TLM calculations and the analytical solutions

The aim is to compare the directional pattern of the scattered field obtained from the TLM calculation with the theory seen in section 3.1.

The scattered pressure level obtained from the TLM calculations are compared to the theoretical scattered level. It is important to keep in mind that TLM simulations presented in this section consider a monochromatic incident plane wave propagated toward a perfectly rigid circular scatterer. Figure 5 shows the polar variation of the scattered pressure field level obtained after the plane wave hit the cylinder (see Fig. 4). Every simulation corresponds to a given frequency of the line source constricted in the frequency range [200 - 1600] Hz.

From figure 5 it can be seen that every simulation the scattered level pattern is in good agreement with the theory. For few angles where the scattered level is highly fluctuating, some of the pattern resulting from the TLM simulations are slightly different compare to the theory. This can be explained by a slight difference between the theoretical receiver positions depicted in figure 4 and there real position on the discretized square TLM network. Moreover, the definition of the circular shape of the scatterer can be altered by the discretization process, i.e. the scatterer is not perfectly circular on its whole circumference. More especially if the scatterer surface is transverse to the TLM-grid the circle is approximated by steps which length is equal to the spatial step. This approximation can explain some of the discrepancies especially at high frequencies. The results shows, however, that the TLM method enables to take into account the scattering of an acoustic wave by a single rigid circular scatterer.

4 Multiple scattering

4.1 Theory from Twersky's average wave-function [8]

In this section, the physical quantity of interest is the mean energy density $|\psi|^2$, extracted from the work of Twersky [9, 10]. Considering an incident plane wave which travels through an array of scatterers. This array can be seen as a linear time-invariant system which can be characterized from the study of the scattering phenomena inside the system. The waves traveling inside the array of scatterers can be split into two parts: one is transmitted to the end of the array and the other is back-scattered. Embleton [8] reminds that such phenomena can expressed with the average wave transmitted T and reflected R [9] given by:

$$T = \frac{2W}{k}\sum_{-\infty}^{\infty} A_n, \tag{15}$$

and

$$R = \frac{2N}{k}\sum_{-\infty}^{\infty}(-1)^n A_n\,, \tag{16}$$

where W is the number of scatterer per square meter, N is the total number of scatterer, k is the wavenumber and the coefficient A_n is given by:

$$A_n = -\frac{iJ_n(kr) + (Z/\rho c)J_n'(kr)}{iH_n(kr) + (Z/\rho c)H_n'(kr)}. \tag{17}$$

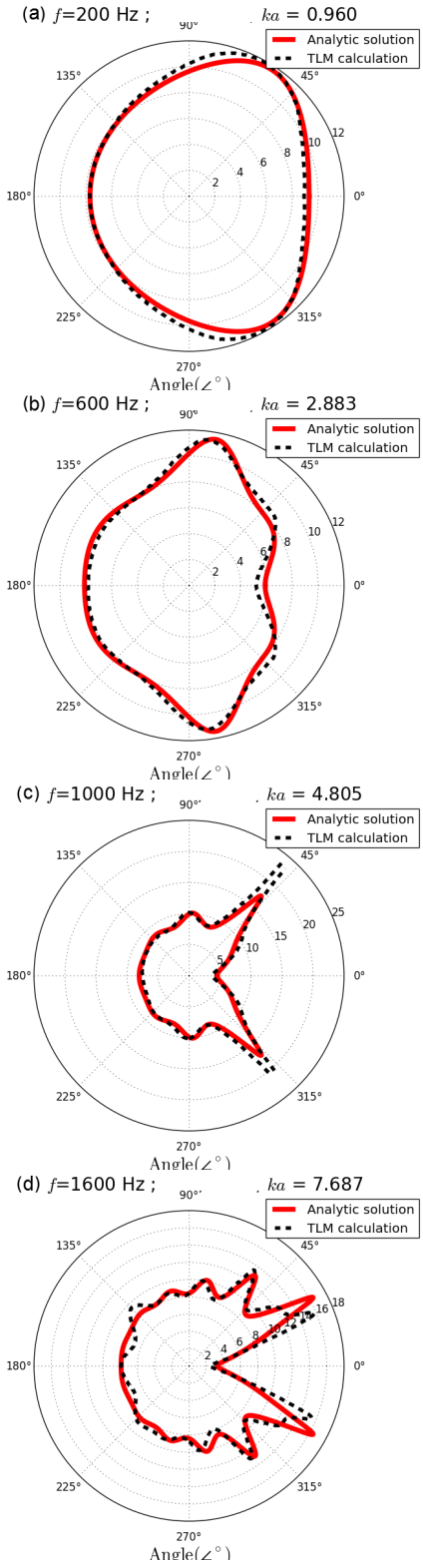

Figure 5: Sound level pressure L for analytic solutions (Bruneau [7]) (red solid line: —) and TLM calculations (black dashes: - -): (a) $ka = 0.960$; (b) $ka = 2.883$; (c) $ka = 4.805$; (d) $ka = 7.687$.

From equations (15) and (16) Twersky [9] defines two quantities γ and q given by:

$$\gamma = \sqrt{(k - iT)^2 + R^2} \tag{18}$$

and

$$q = (T + ik - i\gamma)/R\,, \tag{19}$$

where γ is the complex propagation constant and q corresponds to the balance between the transmitted and back-scattered field. The incident and transmitted wave field are written as:

$$\psi_i = (1 - q)\frac{e^{i\gamma x} + qe^{-i\gamma(x-2d)}}{1 - q^2 e^{i2\gamma d}}, \tag{20}$$

and

$$\psi_t = (1 - q^2)\frac{e^{i(\gamma-k)d}}{1 - q^2 e^{i2\gamma d}}\,, \tag{21}$$

where ψ_i and ψ_t describes respectively the internal and the transmitted wave field. Embleton [8] studied the mean energy loss, which can be written as:

$$EL = 10\log_{10}\left(\frac{|\psi_t|^2}{|\psi_{t,100ft}|^2}\right), \tag{22}$$

where $\psi_{t,100ft}$ is the mean energy density calculated for a scatterers array of 100 feet (30.48 m) length and normalized with respect to $Wa = 10^{-2}\mathrm{m}^{-1}$, where W is the scatterer's density and a the scatterers' radius.

4.2 Numerical results

4.2.1 Geometry of the simulations

TLM calculations are carried out with a sinusoid line source which frequency ranges from 50 Hz to 800 Hz. The transmission-line network is defined as a square lattice which spatial step is set equal to $\delta l = 2.5\ 10^{-2}$ m. This spatial step corresponds to a sampling frequency equivalent to $\lambda/17$ for the maximal frequency 800 Hz.

As shown in figure 6, the computational domain consists mainly of a scatterers area, which is placed between the line source and the line of 10 receivers. The scatterers area is defined by its surface (S_{scat}) *i.e.* the array where the scatterers are located, the radius of the scatterers (a) and the number of scatterer per square meter (W). In the following simulations the 2D computational domain can be seen as a corridor where a line source is placed at the entrance and a line of receivers is located near to the end of the corridor length. Boundaries along the length are perfectly reflecting also named as cyclic boundaries in [11]. Two absorbing layers based on the one-way approach [12] are placed at the entrance and at the very end of the corridor.

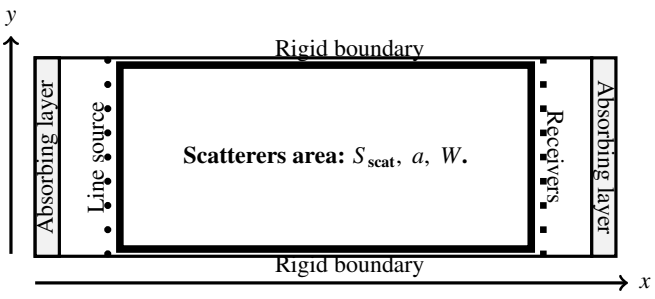

Figure 6: Computational domain of the TLM simulations for the study of multiple scattering.

The complete computational domain is an array of 10 m x 44.5 m. An example of the scatterers area is depicted in the next section (see Fig. 7). The scatterers are randomly distributed within the scatterers area with respect to the Gibbs point process described in the following section. Therefore, the transmission-line network is made

of: $(n_x = 1780) \times (n_y = 400) = 7.12\ 10^5$ nodes. The line source is located at $x = 4$ m along the y-axis and the receivers are located at $x = 34.48$ m parallel to the y-axis (See Fig. 6). This gives a distance between the source and the receivers equal to 30.48 m (100 ft) as used in [8]. The time step for every simulation is $\delta t = 5.4\ 10^{-5}$ s. The simulation duration is $t_{sim} = 0.41$ s. The scatterers are two-dimensional circles which radius is constant and set equal to $a = 0.10$ m. Three scatterers densities W and three area's lengths are tested in the following TLM simulations. The surface of the scatterers is considered as acoustically rigid.

4.2.2 Distribution process for the scatterers locations

The spatial point process model can be seen as a mathematical model which is commonly use for the definition of the trees locations in the study of forests structures. Among the point processes, the Gibbs point process enables to define the interactions between the points from a pair potential function. As an interesting feature for the present study, the Gibbs point process allows to define a "hard-core" condition in order to avoid scatterers superpositions. An example of the scatterers distribution where $Wa = 10^{-2}\text{m}^{-1}$ used as a reference is given in figure 7(a) with the corresponding pair potential function (c). The analysis of the spatial distribution of the scatterers resulting from the point process is carried out with the Ripley function $K(r)$ and the Besag function $L(r)$ (see fig. 7 (c) and (d)). The Ripley function can be written as [13, 15]

$$K(r) = \frac{1}{W}\frac{1}{N}\sum_{i=1}^{N}\sum_{j\neq i} k_{ij}, \tag{23}$$

where W is the density, N is the total number of scatterers, and k_{ij} is equal to 1 if the distance between the points i and j is inferior to r, and zero if not. The Besag function is written [14, 15]

$$L(r) = \sqrt{\frac{K(r)}{\pi}} - r. \tag{24}$$

Both functions got the same information, but in some cases the Besag function can be easier to interpret.

In this work we are interested in distributions where the position of a given point is independent of the other points' distribution. This is the definition of a Poisson's distribution, which is equivalent to the assumption of complete randomness. This distribution is often used as a basic reference in the study of spatial structure of forests [15]. In figure 7(c) and (d) both Ripley and Besag functions are compared to the ideal Poisson's distribution (solid black lines). The edge effect [16] (blue solid lines) has been integrated to the initial calculation (solid red lines) to take into account the divergences of k_{ij} (Eq. (23)) for the points located close to the edges. In figure 7(c) and (d), it can be seen that the corrected values are close to the Poisson process which ensures a random distribution for the distance $r = [0\ ;\ 3.5]$ meters. Every scatterers areas considered in the following sections are defined with respect to this random distribution hypothesis.

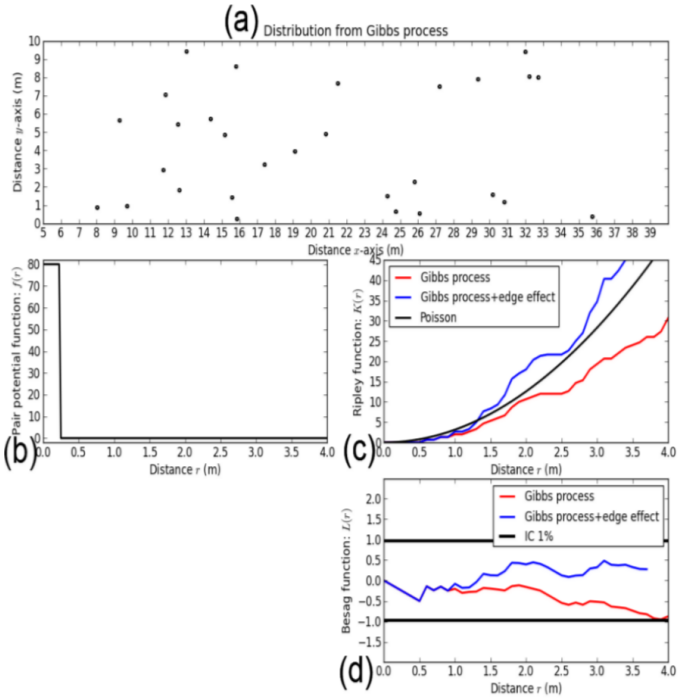

Figure 7: Reference scatterers area for $a = 0.10$m and $Wa = 10^{-2}\text{m}^{-1}$ obtained from the Gibbs process: (a) scatterers area ; (b) pair potential function: $f(r)$; Ripley function: $K(r)$; Besag function: $L(r)$.

4.2.3 Comparison between the TLM calculations and the analytical solutions

Increase of density

The influence of the density is tested using two values of the factor Wa: $Wa = 2.10^{-2}\text{m}^{-1}$ and $Wa = 3.10^{-2}\text{m}^{-1}$. The scatterer radius is set equal to $a = 0.10$ m for every scatterers area. It is important to keep in mind that the scatterers area defined in figure 7 with $Wa = 10^{-2}\text{m}^{-1}$ is used as a reference for the calculation of the attenuations (see Eq. 22). Figure 8 shows a comparison between the attenuation obtained form the TLM calculations and the theoretical attenuations calculated from the section 4.1). It can be seen that for both cases the TLM results are in good agreement with the theory for low values of ka up to $ka = 1$. Above this limit the attenuations are slightly fluctuating around the theoretical curves. From $ka = 1$ the directivity pattern around the circular scatterer is no longer assumed to be omnidirectional. Thus, the initial sound wave is scattered in specific directions and the interactions between every scattered wave become more complex. This induces a larger fluctuation of the pressure at the outside of the scatterers area. Such discrepancies has already been observed in a larger extent from finite-differences time-domain (FDTD) simulations by Heimann for several densities and scatterers' radius [11]. The present results show that the TLM method is in good agreement with the theory for low ka values and corroborates the observations done with the FDTD method.

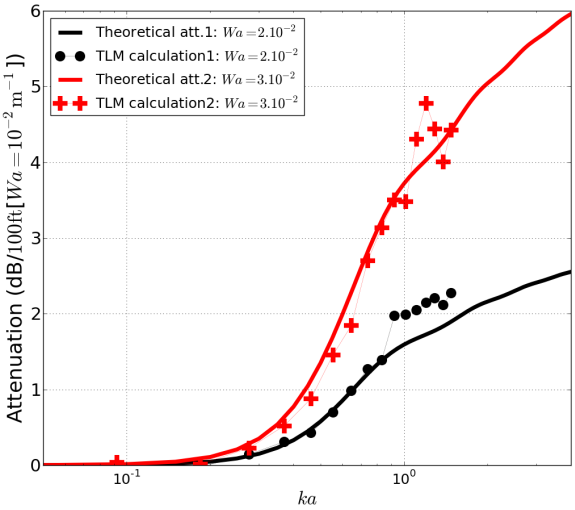

Figure 8: Attenuations calculated with a reference domain where $Wa = 10^{-2}\text{m}^{-1}$ for a scatterers domain where $Wa = 2.10^{-2}\text{m}^{-1}$ (black points), and a scatterers domain where $Wa = 3.10^{-2}\text{m}^{-1}$ (red crosses) in comparison to the corresponding theoretical attenuations.

5 Conclusion

The aim of the present paper is to investigate the TLM method's ability to simulate multiple scattering by tree-trunks that occurs inside forests. As a first step, the scattering of a plane wave on a single circular scatterer has been studied. From the comparison between the TLM simulations and the analytical solutions, it has been shown that the TLM method enables to take into account sound scattering from an acoustically rigid circular cylinder. In the last section, multiple scattering is studied, after discussing the distribution process used for the placement of the scatterers. The acoustic field scattered by an array of randomly placed circular scatterer has been simulated with the TLM method. It has been shown that for two densities the numerical results are in good agreement with the theory for $ka < 1$. Above this limit, the numerical scattered levels are fluctuating around the theoretical values. Such results corroborate the observations done with the FDTD method in [11]. This confirmed the ability of the TLM method to deal with scattering problems. These are encouraging results for the study of forested area using the TLM method.

References

[1] Price, M.; Sound attenuation through trees: measurements and models, *J. Acoust. Soc. Am.*, **84**, 1836 - 1844 (1988).

[2] Renterghem, T. V.; Botteldooren, D.; Verheyen, K.; Road traffic noise shielding by vegetation belts of limited depth, *J. Sound Vib.*, **331**, 2404-2425 (2012).

[3] Tunick, A.; Calculating the micrometeorological influences on the speed of sound through the atmosphere in forests, *J. Acoust. Soc. Am.*, **114**, 1796-1806 (2003).

[4] Guillaume, G.; Picaut, J.; Dutilleux, G.; Gauvreau, B.; Time-domain impedance formulation for transmission line matrix modeling of outdoor sound propagation, *J. Sound Vib.*, 330, 6467-6481 (2011)

[5] Guillaume, G.; Aumond, P.; Gauvreau, B.; Dutilleux, G.; Application of the transmission line matrix method for outdoor sound propagation modelling – Part 1: Model presentation and evaluation, *Appl. Acoust.*, **76**, 113-118 (2014).

[6] Kagawa, Y.; Tsuchiya, T.; Fuji, B.; Fujioka, K.; Discrete Huygen's model approach to sound wave propagation, *J. Sound Vib.*, **218**, 419-444 (1998).

[7] Bruneau, M.; Hermès (Ed.) Manuel d'acoustique fondamentale, Hermès (1998).

[8] Embleton, T.; Scattering by an array of cylinders as a function of surface impedance, *J. Acoust. Soc. Am.*, **40**, 667-670 (1966).

[9] Twersky, V.; On scattering of waves by random distributions. I. Free space scatterer formalism, *J. Math. Phys.*, **3**, 700-715 (1962).

[10] Twersky, V.; Acoustic bulk parameters of random volume distributions of small scatterers *J. Acoust. Soc. Am.*, **36**, 1314-1329 (1964).

[11] Heimann, D.; Numerical simulation of wind and sound propagation through an idealised stand of trees, *Acta Acustica*, **89**, 779-788 (2003).

[12] Guillaume, G; Picaut, J; A simple absorbing layer implementation for transmission line matrix modeling, *J. Sound Vib.*, **332**, 4560-4571 (2013).

[13] Ripley B.; The second order analysis of stationary point process, *Journal of applied probability*, **13**, 255-266 (1976).

[14] Besag J.; Contribution to the discussion of Dr Ripley's paper, *Journal of the royal statistical society*, **B 39**, 193-195 (1977).

[15] Goreaud, F.; Apports de l'analyse de la structure spatiale en forêt tempérée à l'étude et la modélisation des peuplements complexes. Phdthesis, ENGREF (2000).

[16] Goreaud F.; Pélissier R.; On explicit formulas of edge effect correction for Ripley's K-function, *Journal of Vegetation Science*, **10**, 433-438 (1999).